PHYSICAL REVIEW B **96**, 241103(R) (2017)

In-plane magnetization-induced quantum anomalous Hall effect in atomic crystals of group-V elements

Peichen Zhong,[1,2] Yafei Ren,[1,2] Yulei Han,[1,2] Liyuan Zhang,[3,*] and Zhenhua Qiao[1,2,†]

[1]*ICQD, Hefei National Laboratory for Physical Sciences at Microscale, and Synergetic Innovation Center of Quantum Information and Quantum Physics, University of Science and Technology of China, Hefei, Anhui 230026, China*

[2]*CAS Key Laboratory of Strongly-Coupled Quantum Matter Physics, and Department of Physics, University of Science and Technology of China, Hefei, Anhui 230026, China*

[3]*Department of Physics, South University of Science and Technology of China, Shenzhen, Guangdong 518055, China*

(Received 6 June 2017; revised manuscript received 31 October 2017; published 14 December 2017)

We theoretically demonstrate that the in-plane magnetization-induced quantum anomalous Hall effect (QAHE) can be realized in the atomic crystal layers of group-V elements with a buckled honeycomb lattice. Based on sp^3 tight-binding models with parameters being extracted from first-principles results, we show that for weak and strong spin-orbit couplings, the systems harbor QAHEs with Chern numbers of $\mathcal{C} = \pm 1$ and ± 2, respectively. For $\mathcal{C} = \pm 1$ phases, we find the critical magnetization to realize QAHE can be extremely small by tuning the spin-orbit coupling strength. For $\mathcal{C} = \pm 2$ phases, we find that although the critical magnetization is larger, it can be decreased effectively by strain. Moreover, the band gap is large enough for a room-temperature observation. These features suggest that it is experimentally feasible to realize high-temperature QAHEs from in-plane magnetization in the atomic crystal layers of group-V elements.

DOI: 10.1103/PhysRevB.96.241103

Introduction. The past few years have witnessed both theoretical and experimental progresses towards the understanding and realization of the quantum anomalous Hall effect (QAHE) [1], which exhibits insulating bulk and conducting edges where the states are topologically protected from backscattering and show potential applications in low-energy consumption electronics [2–6]. On the experimental side, the QAHE has been observed in magnetically doped three-dimensional (3D) topological-insulator thin films, however, under ultralow temperatures [7–10]. This has further stimulated the search for high-temperature QAHEs in topological thin films, e.g., by considering the charge-compensated n-p codoping mechanism [11]. On the theoretical side, in narrow or zero-gap systems, such as graphene [12–15], silicene [16,17], and other atomic crystal layers [2,18,19], the QAHE has been studied extensively by applying out-of-plane magnetization, which, however, has not yet been observed experimentally.

The realization of QAHE requires the breaking of time-reversal symmetry, which is usually achieved by out-of-plane magnetization. Alternatively, the in-plane one, which is more energetically preferred in magnetic thin films (see Refs. [20,21] and the Supplemental Material [22]), also exhibits the capability to induce QAHE in atomic crystal layers that display broken out-of-plane mirror-reflection symmetry [23,24]. The research on a high-temperature QAHE from in-plane magnetization is still in its infancy [23–25]. A recent experiment has reported the opening of a tiny band gap around 10 meV in Bi thin films [26], the structure of which satisfies the symmetry requirement of harboring QAHEs from in-plane magnetization [27,28]. Its strong spin-orbit coupling (SOC) and tiny bulk gap together suggest a possible large-gap QAHE from weak magnetization.

In this Rapid Communication, we theoretically investigate the possibility of realizing QAHEs from in-plane magnetization in the atomic crystal layers of group-V elements with a buckled honeycomb lattice based on the tight-binding model and first-principles calculations. As concrete examples, we consider two limits of strong and weak SOCs, which correspond respectively to a $\mathbb{Z}_2$ topological insulator and a topologically trivial band insulator in the absence of magnetization. By applying in-plane magnetization, we find that QAHEs can be realized in both cases to exhibit Chern numbers of $\mathcal{C} = \pm 2$ and ± 1, separately. We then systematically study the phase diagram by manipulating the SOC strength, magnetization magnitude, and its orientation. The former case exhibits a topologically nontrivial band gap that is much larger than the room-temperature energy. Moreover, the critical magnetization can be effectively reduced by applying strain. For the latter case, the critical magnetization depends highly on the SOC strength and can even reach close to zero. The resulting tiny topological band gap can be enlarged by orders through slightly tilting the magnetization orientation from in plane.

Model Hamiltonian. The tight-binding Hamiltonian is constructed by employing the two-center approximation on the orthogonal basis of $\{|s\rangle,|p_x\rangle,|p_y\rangle,|p_z\rangle\} \otimes \{|\uparrow\rangle,|\downarrow\rangle\}$ [29,30],

$$H = \sum_{i\alpha} \epsilon_\alpha c_{i\alpha}^\dagger c_{i\alpha} - \sum_{i\alpha,j\beta} t_{ij,\alpha\beta} c_{i\alpha}^\dagger c_{j\beta} + t_{\mathrm{SO}} \sum_i c_{i\alpha}^\dagger \boldsymbol{l} \cdot \boldsymbol{s} c_{i,\beta} + \lambda \sum_{i\alpha} c_{i\alpha}^\dagger \hat{\boldsymbol{m}} \cdot \boldsymbol{s} c_{i\alpha}, \quad (1)$$

where $c_{i\alpha}^\dagger = (c_{i\alpha\uparrow}^\dagger, c_{i\alpha\downarrow}^\dagger)$ is the creation operator of an electron at the ith atomic site with $\uparrow$ / $\downarrow$ and α/β representing spin up/down and different orbitals, respectively. The first term is the on-site energy, which is degenerate for p_x and p_y orbitals due to threefold rotation symmetry. The second term stands for the hopping energy up to next-nearest neighbors

*Corresponding author: zhangly@sustc.edu.cn
†Corresponding author: qiao@ustc.edu.cn

TABLE I. Slater-Koster tight-binding parameters of a Bi (111) bilayer with a lattice constant $a = 4.39$ Å and interlayer distance $d = 1.73$ Å in the absence of SOC. Unit: eV. The unprimed and primed parameters correspond to nearest- and next-nearest-neighbor hoppings, separately.

ϵ_s	$\epsilon_{px,py}$	ϵ_{pz}	$V_{ss\sigma}$	$V_{sp\pi}$	$V_{pp\sigma}$	$V_{pp\pi}$	$V'_{pp\sigma}$	$V'_{pp\pi}$
−8.90	−0.39	−0.41	−0.65	1.94	1.90	−0.55	0.60	−0.20

with an amplitude of $t_{ij,\alpha\beta}$, which are functions of the Slater-Koster parameters listed in Table I [30]. The third term represents the intra-atomic SOC of strength $t_{\rm SO}$ with $\boldsymbol{s} = (s_x, s_y, s_z)$ and $\boldsymbol{l} = (l_x, l_y, l_z)$ being, respectively, the Pauli matrices and orbital-angular-momentum operators. This term can be expressed explicitly as

$$H_{\rm SO} = t_{\rm SO} \begin{pmatrix} 0 & 0 & 0 & 0 \\ 0 & 0 & -is_z & is_y \\ 0 & is_z & 0 & -is_x \\ 0 & -is_y & is_x & 0 \end{pmatrix}. \tag{2}$$

The last term corresponds to an exchange coupling between the electron and magnetization that is defined as $(m_x, m_y, m_z) \doteq \lambda \hat{\boldsymbol{m}} = \lambda(\sin\theta\cos\phi, \sin\theta\sin\phi, \cos\theta)$, where λ is the magnetization strength and θ/ϕ are polar/azimuthal angles. This tight-binding model is generally valid for lattices with s and p orbitals. Without loss of generality, we perform our numerical study by employing the parameters of a Bi (111) bilayer as listed in Table I. These parameters that are extracted from first-principles calculations by using nonlinear least-squares fitting and the electronic structures from this model exhibit quantitative agreement with the first-principles results (see the Supplemental Material for details). In addition, we also consider the effect of biaxial strain that enlarges the lattice constants and reduces the interlayer distance according to the Poisson's ratio that is set to be 0.335 [31]. The Slater-Koster hopping parameters are assumed to exhibit inverse square dependence on the interatomic distance [30].

Band structure. Based on the Hamiltonian, band structures can be obtained as shown in Fig. 1. In the absence of magnetization, Figs. 1(a) and 1(e) display, respectively, the band structures for $t_{\rm SO} = 0.55$ and 0.20 eV, where even and odd parities of wave functions at the time-reversal invariant momenta (Γ and M points) are labeled as "+/−." As a comparison, one can see that the parities of the conduction and valence bands exchange at the Γ point, indicating a topological phase transition from a $\mathbb{Z}_2$ topological insulator to a topologically trivial band insulator [32], which is consistent with previous works [33,34]. We then apply the in-plane magnetization ($\theta = \pi/2$) along the x axis ($\phi = 0$), which meets the symmetry criteria of breaking all the mirror-reflection symmetries of the buckled honeycomb lattice [23,24]. The presence of magnetization breaks the time-reversal symmetry and thus the $\mathbb{Z}_2$ topological phase.

For strong SOC, we find that the increase of λ shrinks the band gap and closes it at $\lambda = 0.64$ eV, as indicated in Fig. 1(b), where a Dirac cone appears on the highly symmetric line M-Γ. It is noteworthy that another Dirac cone also appears (not shown) due to the inversion symmetry of this system. A further increase of λ reopens the band gap, inducing a QAHE with a Chern number of $\mathcal{C} = -2$ obtained by integrating the Berry curvature over the first Brillouin zone according to the formula [35]

$$\mathcal{C} = \frac{1}{2\pi} \sum_n \int_{\rm BZ} d^2k \Omega_n(\boldsymbol{k}), \tag{3}$$

where $\Omega_n(\boldsymbol{k})$ is the Berry curvature at momentum $\boldsymbol{k}$ of the nth band [12,35]. The summation of n runs over all occupied bands below the Fermi energy. In Fig. 1(d), we plot the Berry curvature $\Omega(\boldsymbol{k})$ obtained by summing over all occupied bands, where two negative peaks appear at the highly symmetric line M-Γ-M. The Berry curvature near each peak contributes to a Chern number of -1, resulting in a total Chern number of $\mathcal{C} = -2$.

The realization of QAHE does not necessarily require a $\mathbb{Z}_2$ topological insulator. For a weak SOC case where the bands are topologically trivial [see Fig. 1(e)], the presence of in-plane magnetization can also close the band gap, as shown in Fig. 1(f), where a Dirac cone appears at the Γ point. By further increasing λ, the system harbors a QAHE with a Chern number $\mathcal{C} = 1$ [see Fig. 1(g)]. The corresponding Berry curvature centers around the Γ point with a high peak as plotted in Fig. 1(h).

Phase diagram versus SOC strength and magnetization orientation. The influence of SOC strength $t_{\rm SO}$ on the Chern number is explored systematically in the phase space of $(t_{\rm SO}, \lambda)$, as displayed in Fig. 2(a), where the direct band gap is shown in color. At vanishing magnetization, i.e., $\lambda = 0$, one can see that the band gap first closes and then reopens with an increase of $t_{\rm SO}$, indicating a topological phase transition from a trivial band insulator to a $\mathbb{Z}_2$ topological insulator at the critical point $t^{\rm c}_{\rm SO} \simeq 0.36$ eV. For $t_{\rm SO} > t^{\rm c}_{\rm SO}$, the presence of magnetization generally induces $\mathcal{C} = -2$ QAHE at a relatively large magnetization strength λ. In this regime, one can see that the direct QAHE gap can be very large. In the Supplemental Material, we also present the phase diagram of the indirect band gap. Although the indirect band gap is smaller, it is still in the order of 0.1 eV, which is much larger than the energy scale of room temperature and thus provides the possibility of realizing a high-temperature QAHE.

For $t_{\rm SO} \lesssim t^{\rm c}_{\rm SO}$, the introduction of in-plane magnetization can induce a QAHE phase of a Chern number $\mathcal{C} = 1$. The critical magnetization strength λ_c shows a strong dependence on $t_{\rm SO}$ and decreases to zero as it approaches $t^{\rm c}_{\rm SO}$. As the magnetization strength increases, one can find various topological phase transitions to QAHEs with Chern numbers $\mathcal{C} = -1$, 2, and 0 in sequence. Comparing to the $\mathcal{C} = 1$ phase, these phases have a smaller phase space and require a larger magnetization strength. It is noteworthy that despite the SOC strength in the order of 0.1 eV, the band gap of $\mathcal{C} = 1$ QAHE is rather small. This can be understood from the evolution of energy levels at the Γ point as λ increases, as shown in Fig. 2(b), where the height of the white regime represents the band gap. In the absence of magnetization, i.e., $\lambda = 0$, the conduction band minimal (C_M) and valence band maximal (V_M) are doubly degenerate. As λ increases, the degeneracies are lifted, as shown by the red dashed lines and blue solid

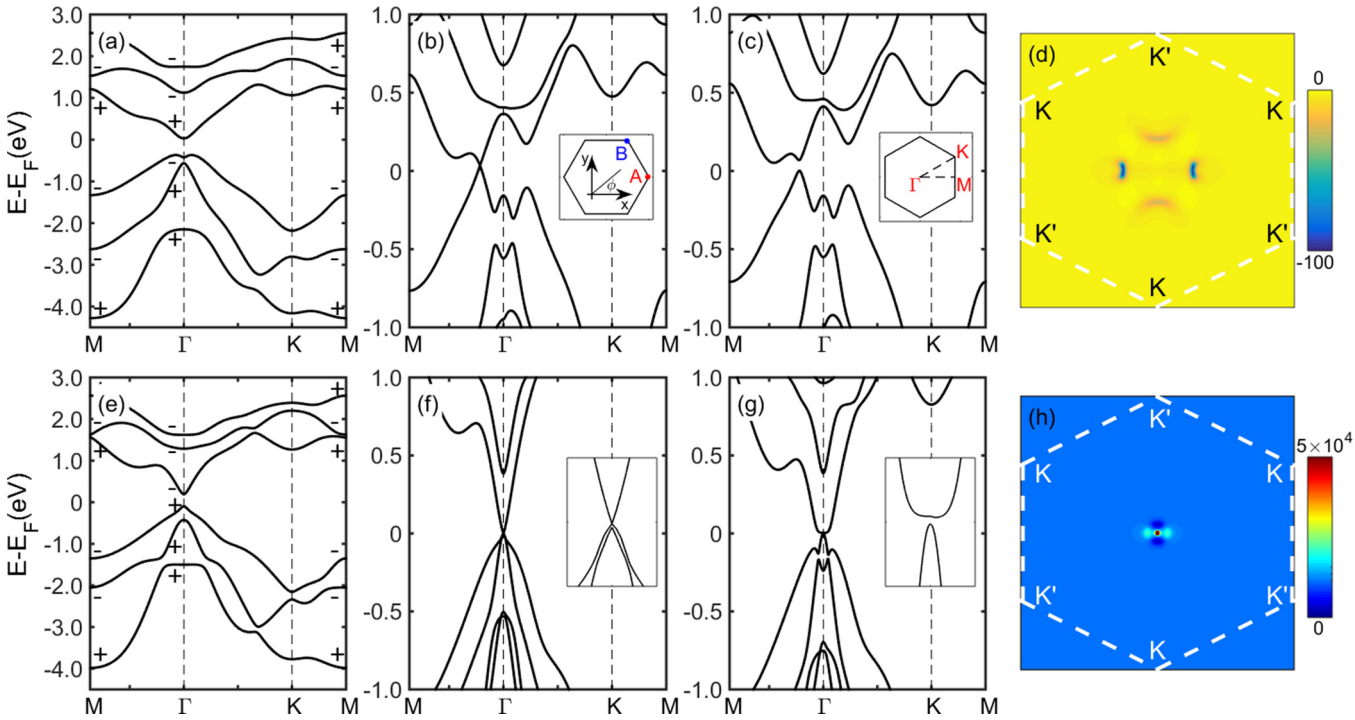

FIG. 1. Band structure vs magnetization strength λ at SOC strengths of (a)–(c) $t_{SO} = 0.55$ eV and (e)–(g) $t_{SO} = 0.2$ eV. (a) and (e) Vanishing magnetization with $\lambda = 0$. Even and odd parities of different eigenstates at time-reversal invariant points (Γ and M) are denoted by $+/-$. The parities of the conduction and valence bands exchange at Γ for these two cases, suggesting a phase transition from (a) a $\mathbb{Z}_2$ topological insulator to (e) a topologically trivial band insulator. (b) and (f) Band structures at topological phase transition points with a closing band gap when (b) $\lambda = 0.64$ eV and (f) $\lambda = 0.205$ eV. (c) and (g) Band structure with a reopened band gap when (c) $\lambda = 0.7$ eV and (g) $\lambda = 0.36$ eV. (d) and (h) Berry curvature distributions for band structures in (c) and (g), which contribute to Chern numbers of $\mathcal{C} = -2$ and $+1$, separately. Inset in (b): Coordinate system and lattice structure with the A (B) sublattice locating on the top (bottom) layer. Inset in (c): Schematic plot of first Brillouin zone and highly symmetric lines. Insets in (f) and (g): Zoom in of band structures near the band closing points. The magnetization is along the x direction with $\theta = \pi/2$ and $\phi = 0$.

lines separately, which shrinks the band gap to zero. After the intersection between the red dashed and blue solid lines, the two states represented by blue lines become separately conduction band minimal and valence band maximum with a small band gap (see more details in the Supplemental Material).

The resulting QAHE is robust when the magnetization changes in the m_x-m_y plane, as shown in Figs. 2(c) and 2(d) for different SOCs $t_{SO} = 0.2$ and 0.55 eV, separately. One can find that both phase diagrams show threefold rotation symmetry since the magnetization orientations along $\phi + 2n\pi/3$ with integer n are equivalent and give rise to the same topological

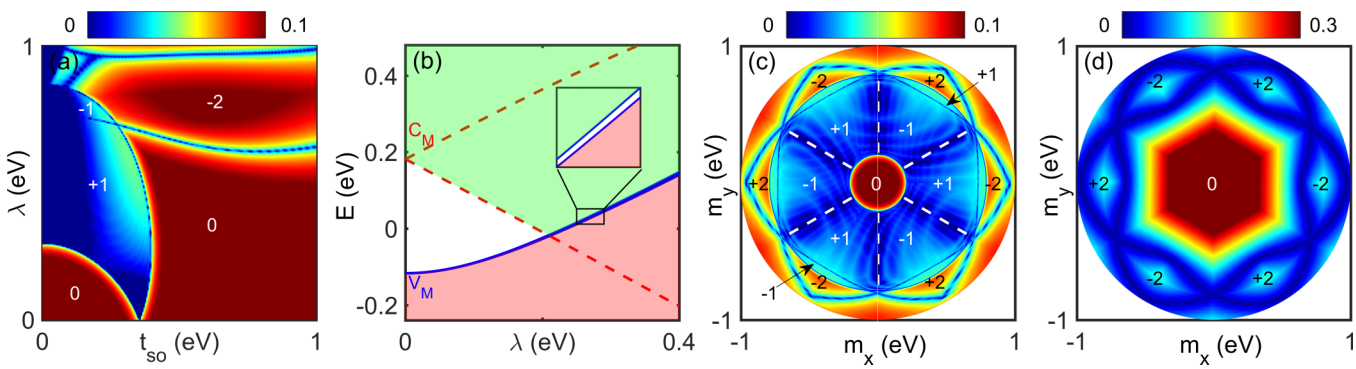

FIG. 2. (a) Phase diagram vs SOC strength t_{SO} and in-plane magnetization magnitude λ. The direct band gap is shown in color in units of eV. The Chern number of each topological phase is shown. (b) Evolution of energy levels at Γ as a function of magnetization λ. The height of the white regime represents the direct band gap at the Γ point for different λ. Above (below) is the energy regime without (with) electron occupation as denoted by light green (red). Red dashed lines and blue solid lines: Different energy levels at the Γ point. C_M and V_M are conduction band minimal and valence band maximal at $\lambda = 0$. (c) and (d) Phase diagram for different in-plane magnetizations in the m_x-m_y plane for (c) $t_{SO} = 0.2$ eV and (d) 0.55 eV.

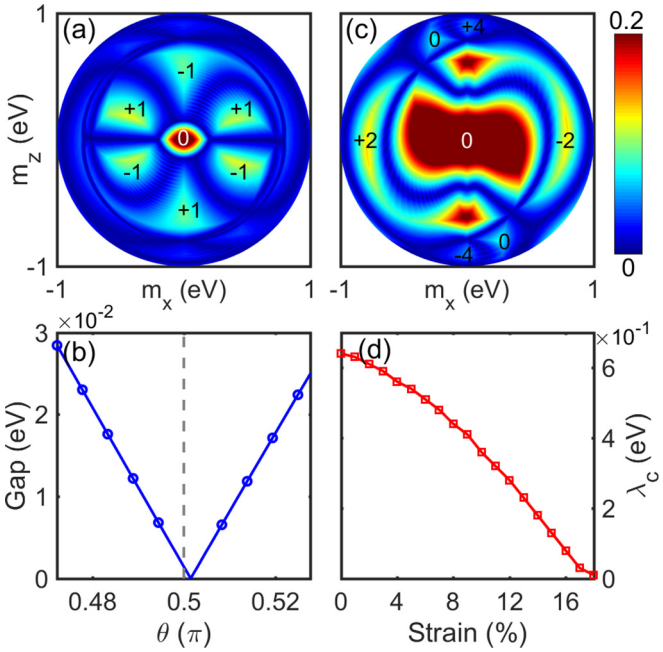

FIG. 3. (a) and (c) Phase diagrams vs m_x-m_z with SOC of (a) $t_{SO} = 0.2$ eV and (c) 0.55 eV. The direct band gap is shown in color in units of eV. (b) Direct band gap vs polar angle θ with $\lambda = 0.36$ eV. (d) Direct band gap vs biaxial strain for $t_{SO} = 0.55$ eV with magnetization pointing along x axis.

phases due to the threefold rotation symmetry of pristine Bi (111) bilayers. When the magnetization is along $\phi = \pi/6 + 2n\pi/3$, which preserves the mirror-reflection symmetry of Bi, no QAHE appears and the band gap is either vanishing or topologically trivial. This is similar to that of silicene and agrees with the symmetry analysis discussed in Ref. [23]. Nevertheless, compared to silicene [23], the critical magnetizations required to reach QAHE for both $t_{SO} = 0.2$ and 0.55 eV are much smaller and experimentally achievable. One can further manipulate the critical magnetization and band gap by changing the SOC strength via alloying with Sb and P [18].

External manipulations. Experimentally, various methods can be employed to induce magnetization in nonmagnetic systems, such as employing transition-metal adatoms or magnetic substrates [13,15,36,37]. These external means might introduce out-of-plane components or strain on the Bi system. In this part, we present the effects of these factors. We find that although the QAHE phase with $\mathcal{C} = \pm 1$ exhibits a tiny bulk band gap, it can be increased effectively by introducing a magnetization component along the z direction. In Fig. 3(a), we plot the direct band gap for different magnetizations in the m_x-m_z plane at a fixed SOC $t_{SO} = 0.2$ eV. One can find that the tilting of magnetization from the x direction to either $+z$ or $-z$ can enlarge the band gap dramatically but with different Chern numbers. Specifically, by changing the magnetization from the x axis ($\theta = \pi/2$) to the z axis, the gap is increased by one order for a variation of θ by only 0.02π, as plotted in Fig. 3(b). When the magnetization is rotated to the $-z$ direction, however, the band gap first closes and then reopens, inducing a phase transition to a QAHE of $\mathcal{C} = -1$. The critical angle is around $(0.5 + 0.0014)\pi$ and a band gap of about 20 meV can be found through changing θ by only 0.02π, similar to the $\mathcal{C} = 1$ case.

For a strong SOC case, such a sensitivity of the topological phase to θ is absent, as shown in Fig. 3(c). From this figure, one can find that the tilting of magnetization orientation from in plane can also close the band gap and induce a topological phase transition to either a topologically trivial band insulator or a QAHE with opposite Chern numbers. However, the critical angle is quite large, indicating the robustness of the QAHE from in-plane magnetization. Although the critical magnetization λ_c is larger, as shown in Fig. 3(d), we find that it can be reduced effectively even close to zero by applying strain, which exists inevitably when Bi is placed on top of certain substrates [38].

Summary and discussion. In summary, by applying in-plane magnetization, we confirmed theoretically the presence of a QAHE in the atomic crystal layers of group-V elements with a buckled honeycomb lattice based on the sp^3 Slater-Koster tight-binding model with parameters being extracted from first-principles calculations. We find that, starting from a topologically trivial band insulator, a QAHE of Chern numbers $\mathcal{C} = \pm 1$ is formed with a small band gap, which can be enlarged effectively by orders via slightly tilting the magnetization from in plane. For a $\mathbb{Z}_2$ topological insulator, the in-plane magnetization can induce a QAHE of Chern number $\mathcal{C} = \pm 2$ with a large band gap that is much bigger than the room-temperature energy scale. Although the critical magnetization strength is also larger, it can be reduced effectively by strain, which appears naturally in the presence of a substrate. This feature strongly benefits the experimental realization of QAHEs in Bi (111) bilayers.

Although our numerical calculations are performed based on the orbital parameters of Bi, the model is general and can capture the qualitative properties of the electronic structures of Sb, As, and P with buckled honeycomb lattices by changing the SOC strength, which suggests that the atomic layers of group-V elements are potential candidates to harbor QAHEs from in-plane magnetization. In addition, these elements also exhibit stable puckered structures [39] or other lattice structures [40] that all satisfy the symmetry criteria. Moreover, for these structures, it has been reported that strain, electric field, or increasing system thickness can reduce effectively their band gap [26,38,41–45], suggesting the possibility of realizing QAHEs with weaker magnetization. Further explorations on inducing in-plane ferromagnetism from adatoms or substrates from first-principles calculations is still desired to provide more detailed suggestions for experimental realizations.

Acknowledgments. We are grateful for the financial support from National Key R & D Program (2016YFA0301700), NNSFC (11474265), and the China Government Youth 1000-Plan Talent Program. L.Z. is supported by Innovation Program of Guangdong (608225320279) and Shenzhen Peacock Program (KQTD2016022619565991). The Supercomputing Center of USTC is gratefully acknowledged for high-performance computing assistance.

[1] F. D. M. Haldane, Phys. Rev. Lett. **61**, 2015 (1988).
[2] Y. F. Ren, Z. H. Qiao, and Q. Niu, Rep. Prog. Phys. **79**, 066501 (2016).
[3] X. Kou, Y. Fan, M. Lang, P. Upadhyaya, and K. L. Wang, Solid State Commun. **215**, 34 (2015).
[4] J. Wang, B. Lian, and S. C. Zhang, Phys. Scr. **2015**, 014003 (2015).
[5] C. X. Liu, S. C. Zhang, and X. L. Qi, Annu. Rev. Condens. Matter Phys. **7**, 301 (2016).
[6] H. Weng, R. Yu, X. Hu, X. Dai, and Z. Fang, Adv. Phys. **64**, 227 (2015).
[7] C. Z. Chang, J. Zhang, X. Feng, J. Shen, Z. Zhang, M. Guo, K. Li, Y. Ou, P. Wei, L. L. Wang, Z. Q. Ji, Y. Feng, S. Ji, X. Chen, J. Jia, X. Dai, Z. Fang, S. C. Zhang, K. He, Y. Wang, L. Lu, X. C. Ma, and Q. K. Xue, Science **340**, 167 (2013).
[8] J. G. Checkelsky, R. Yoshimi, A. Tsukazaki, K. S. Takahashi, Y. Kozuka, J. Falson, M. Kawasaki, and Y. Tokura, Nat. Phys. **10**, 731 (2014).
[9] X. Kou, S. T. Guo, Y. Fan, L. Pan, M. Lang, Y. Jiang, Q. Shao, T. Nie, K. Murata, J. Tang, Y. Wang, L. He, T. K. Lee, W. L. Lee, and K. L. Wang, Phys. Rev. Lett. **113**, 137201 (2014).
[10] C. Z. Chang, W. Zhao, D. Y. Kim, H. Zhang, B. A. Assaf, D. Heiman, S. C. Zhang, C. Liu, M. H. W. Chan, and J. S. Moodera, Nat. Mater. **14**, 473 (2015).
[11] S. Qi, Z. Qiao, X. Deng, E. D. Cubuk, H. Chen, W. Zhu, E. Kaxiras, S. B. Zhang, X. Xu, and Z. Zhang, Phys. Rev. Lett. **117**, 056804 (2016).
[12] Z. H. Qiao, S. A. Yang, W.-X. Feng, W.-K. Tse, J. Ding, Y. G. Yao, J. Wang, and Q. Niu, Phys. Rev. B **82**, 161414(R) (2010).
[13] J. Ding, Z. Qiao, W. Feng, Y. Yao, and Q. Niu, Phys. Rev. B **84**, 195444 (2011).
[14] H. Zhang, C. Lazo, S. Blügel, S. Heinze, and Y. Mokrousov, Phys. Rev. Lett. **108**, 056802 (2012).
[15] Z. Qiao, W. Ren, H. Chen, L. Bellaiche, Z. Zhang, A. H. MacDonald, and Q. Niu, Phys. Rev. Lett. **112**, 116404 (2014).
[16] M. Ezawa, Phys. Rev. B **87**, 155415 (2013).
[17] H. Pan, Z. Li, C. C. Liu, G. Zhu, Z. Qiao, and Y. Yao, Phys. Rev. Lett. **112**, 106802 (2014).
[18] H. Zhang, F. Freimuth, G. Bihlmayer, S. Blügel, and Y. Mokrousov, Phys. Rev. B **86**, 035104 (2012).
[19] H. Zhang, F. Freimuth, G. Bihlmayer, M. Ležaić, S. Blügel, and Y. Mokrousov, Phys. Rev. B **87**, 205132 (2013).
[20] M. Stampanoni, A. Vaterlaus, M. Aeschlimann, and F. Meier, Phys. Rev. Lett. **59**, 2483 (1987).
[21] C. A. F. Vaz, J. A. C. Bland, and G. Lauhoff, Rep. Prog. Phys. **71**, 056501 (2008).
[22] See Supplemental Material at http://link.aps.org/supplemental/10.1103/PhysRevB.96.241103 for a detailed description of our related first principles' calculations [46–48] and results on direct and indirect band gaps [49,50].
[23] Y. Ren, J. Zeng, X. Deng, F. Yang, H. Pan, and Z. Qiao, Phys. Rev. B **94**, 085411 (2016).
[24] X. Liu, H.-C. Hsu, and C.-X. Liu, Phys. Rev. Lett. **111**, 086802 (2013).
[25] X.-L. Sheng and B. K. Nikolić, Phys. Rev. B **95**, 201402 (2017).
[26] S. Ito, B. Feng, M. Arita, A. Takayama, R.-Y. Liu, T. Someya, W.-C. Chen, T. Iimori, H. Namatame, M. Taniguchi, C.-M. Cheng, S.-J. Tang, F. Komori, K. Kobayashi, T.-C. Chiang, and I. Matsuda, Phys. Rev. Lett. **117**, 236402 (2016).
[27] D. Hou, Z. Qiu, K. Harii, Y. Kajiwara, K. Uchida, Y. Fujikawa, H. Nakayama, T. Yoshino, T. An, K. Ando, X. Jin, and E. Saitoh, Appl. Phys. Lett. **101**, 042403 (2012).
[28] S. Xiao, D. Wei, and X. Jin, Phys. Rev. Lett. **109**, 166805 (2012).
[29] Y. Liu and R. E. Allen, Phys. Rev. B **52**, 1566 (1995).
[30] W. A. Harrison, *Elementary Electronic Structure* (World Scientific, Singapore, 1999).
[31] http://www.azom.com/properties.aspx?ArticleID=590
[32] L. Fu and C. L. Kane, Phys. Rev. B **76**, 045302 (2007).
[33] S. Murakami, Phys. Rev. Lett. **97**, 236805 (2006).
[34] Y. M. Koroteev, G. Bihlmayer, E. V. Chulkov, and S. Blügel, Phys. Rev. B **77**, 045428 (2008).
[35] D. Xiao, M.-C. Chang, and Q. Niu, Rev. Mod. Phys. **82**, 1959 (2010).
[36] Z. Wang, C. Tang, R. Sachs, Y. Barlas, and J. Shi, Phys. Rev. Lett. **114**, 016603 (2015).
[37] C. Tang, B. Cheng, M. Aldosary, Z. Wang, Z. Jiang, K. Watanabe, T. Taniguchi, M. Bockrath, and J. Shi, APL Mater. **6**, 026401 (2018).
[38] Z.-Q. Huang, F.-C. Chuang, C.-H. Hsu, Y.-T. Liu, H.-R. Chang, H. Lin, and A. Bansil, Phys. Rev. B **88**, 165301 (2013).
[39] G. Wang, R. Pandey, and S. P. Karna, ACS Appl. Mater. Interfaces **7**, 11490 (2015).
[40] F. Ersan, E. Aktürk, and S. Ciraci, Phys. Rev. B **94**, 245417 (2016).
[41] C. Kamal and M. Ezawa, Phys. Rev. B **91**, 085423 (2015).
[42] Q. Liu, X. Zhang, L. B. Abdalla, A. Fazzio, and A. Zunger, Nano Lett. **15**, 1222 (2015).
[43] D. Wang, L. Chen, H. Liu, and X. Wang, Europhys. Lett. **104**, 57011 (2013).
[44] Z. Liu, C.-X Liu, Y.-S. Wu, W.-H. Duan, F. Liu, and J. Wu, Phys. Rev. Lett. **107**, 136805 (2011).
[45] H. W. Yeom, K.-H. Jin, and S.-H. Jhi, Phys. Rev. B **93**, 075435 (2016).
[46] P. E. Blöchl, Phys. Rev. B **50**, 17953 (1994).
[47] G. Kresse and J. Furthmuller, Phys. Rev. B **54**, 11169 (1996).
[48] J. P. Perdew, J. A. Chevary, S. H. Vosko, K. A. Jackson, M. R. Pederson, D. J. Singh, and C. Fiolhais, Phys. Rev. B **46**, 6671 (1992)
[49] Y. Ren, X. Deng, J. Zeng, T. Hou, and Z. Qiao (unpublished).
[50] R. Winkler, *Spin-Orbit Coupling Effects in Two-Dimensional Electron and Hole Systems* (Springer, Berlin, 2003).